5.9 Medical Application/Imaging

Over the past five years, the research field of X-ray imaging has advanced greatly. In particular, X-ray phase-contrast imaging methods such as X-ray inteferometer phase-contrast CT, X-ray diffraction enhanced imaging and X-ray coherent diffraction microscopy have been developed remarkably. Research into polarization-contrast imaging using the polarisation features of synchrotron radiation has also steadily developed. Following improvements to the two-dimensional imaging system for intravenous coronary angiography which is unique to Japan, along with the high current and the long lifetime of the Photon Factory electron beam obtained by efforts of the accelerator group, more practical clinical examinations are being carried out at present. We plan to continue this project for clinical evaluation.In the near future, enormous progress is expected in the research field of X-ray imaging, including clinical applications.

5-9-1 X-ray phase-contrast imaging

When X-rays propagate through an object, the wave-front of the X-rays is deformed due to the phase-shifts caused by the object. X-ray phase-contrast imaging detects these phase-shifts for observing the inner structures of various objects non-destructively [1-2]. Because the sensitivity of X-ray phase-contrast imaging is much higher than that of absorption-contrast imaging, efforts have been made throughout the world into the R&D of this innovative technique. At the Photon Factory techniques such as X-ray interferometry, X-ray diffraction enhanced imaging (DEI), and X-ray coherent diffraction microscopy (XCD) have been pursued intensively.

X-ray phase-contrast CT using an X-ray interferometer

X-ray phase-contrast CT using an X-ray interferometer was first developed at BL-14B in 1996 [3]. At that time, the field-of-view was about 15 mm (V) × 10 mm (H) in size due to the limited size of the beam and interferometer. To enlarge the field-of-view, (i) activities were moved from BL-14B to BL-14C1 and (ii) large-size X-ray interferometers were produced. Figure 1(a) shows an X-ray imaging system with a two-crystal interferometer [4]. The size of the field-of-view is about 25 mm (V) × 30 mm for 35 keV X-rays. Figure 1(b) shows an in-vivo phase-contrast X-ray CT image of a cancer implanted in a nude mouse. The location and structure of a colon cancer, the thin muscle layer, and the cancer lesion are clearly seen. This result demonstrates that X-ray interferometers might be used to observe in-vivo biological objects for future biomedical research.

X-ray diffraction enhanced imaging (DEI)

X-ray diffraction enhanced imaging (DEI) detects slight changes in X-ray propagation directions caused by an object (Fig. 2(a)) [5-6]. Because the analyzer

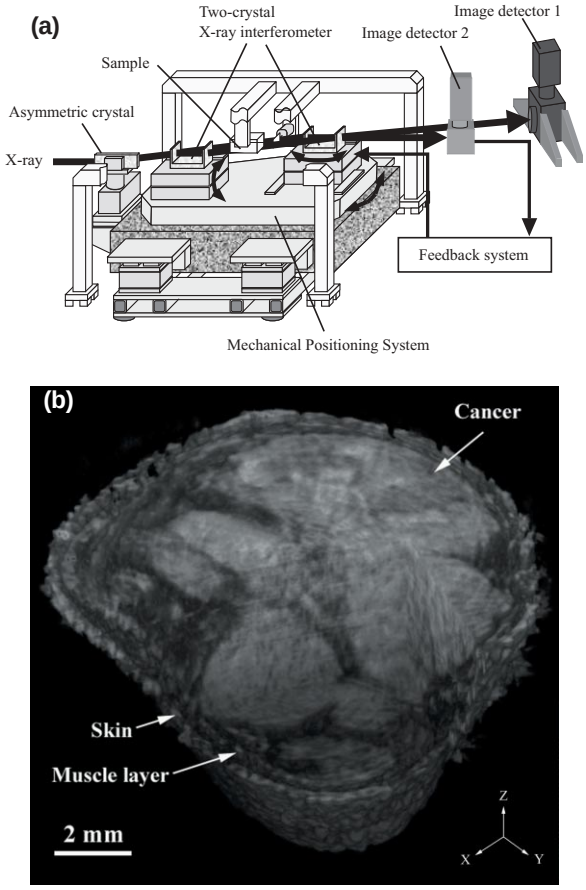

Figure 1
(a) Schematic view of phase-contrast X-ray imaging system based on a two-crystal X-ray interferometer [4]. (b) Three-dimensional in-vivo phase-contrast X-ray CT image of a colon cancer implanted in a nude mouse [4].

plays a key role in DEI, investigation of the analyzer has been carried out at BL-14B, BL-14C and BL-15C. For example, a Laue-case analyzer was developed [7-8] and applied todark-field imaging of the human joint structure [9]. Another example is a resolution-tunable double-crystal analyzer, which allows us to observe a wide variety of samples with the same optics [10]. By combining DEI and CT, 3D phase-contrast images of an object can be obtained [11]. At BL-14B, DEI-CT has been investigated by two groups [12-13]. For example, Fig. 2(b) shows a reconstructed 3D image of an ant obtained with 20.7 keV X-rays [13]

X-ray coherent diffraction microscopy (XCD)

X-ray coherent diffraction microscopy (XCD) is a powerful technique for obtaining 2D and 3D images of non-periodic objects [14]. It is expected that the combination of this technique and next generation light sources such as XFEL and ERL will make it possible to observe single bio-molecules at atomic resolution [15]. Although it is difficult to perform XCD experiments at the Photon Factory due to low beam intensity, simulations have shown that elemental mapping can be realized by making use of anomalous dispersion around absorption edges [16].

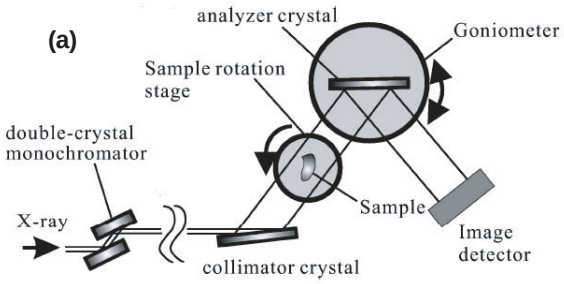

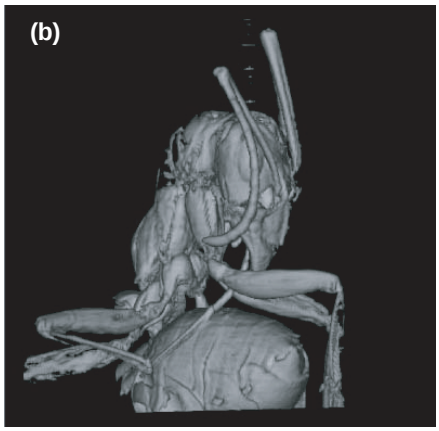

Figure 2
(a) Typical X-ray optics for DEI experiment [12]. (b) 3D reconstructed phase-contrast image of an ant [12].

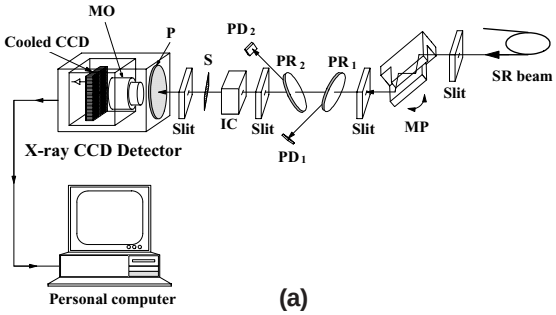

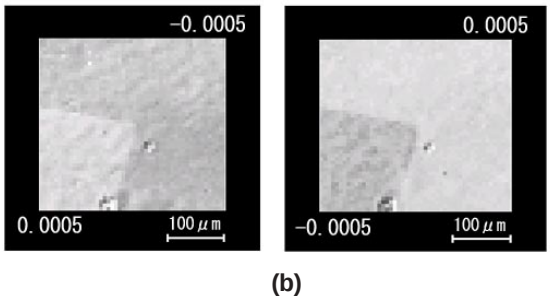

Figure 3
(a) Experimental setup for acquiring images resulting from X-ray magnetic linear dichroism (XMLD) [18]. (b) Images resulting from the X-ray magnetic linear dichroism (XMLD) in the sample. The view field is 303 μm × 317 μm in size [18].

5-9-2 X-ray polarization-contrast imaging

The development of X-ray phase retarders in the transmission geometry in 1991 [17] opened up a new possibility of performing polarization-contrast imaging in the hard X-ray energy region. For example, Fig. 3(a) shows an imaging system consisting of an X-ray polarizer, double diamond phase retarders, and an X-ray CCD detector [18]. This system was used for observing magnetic domains on magnetic tape (Fig. 3(b)). The contrast was produced by the effect of X-ray magnetic linear dichroism (XMLD). Although the XMLD signal is small (about 0.0006 in the relative absorption difference), the magnetic domains are discernible.

5-9-3 Various X-ray imaging methods

Micro-angiography

Using conventional angiographic systems it is not possible to identify peripheral arteries of less than 200 microns in diameter. However, applying a new angiographic system using monochromatic synchrotron radiation with a high-definition CCD video camera system, we have been successful in identifying arteries as small as 50 microns. Microangiography was performed with rats, studying hind limbs in vivo and hearts using the Langendorff perfusion apparatus. Morphological changes in the peripheral and coronary arteries were investigated under physical and pharmacological vasoactive interventions. With the use of a potassium channel blocker, coronary blood flow decreased to less than half of the normal value determined using a Langendorff perfusion apparatus. Using microangiography by synchrotron radiation, vasospasms were observed at the main branches of the coronary artery (Fig. 4). The pathogenesis of the coronary spasm was explained either by hypercontraction of the vascular smooth vas-

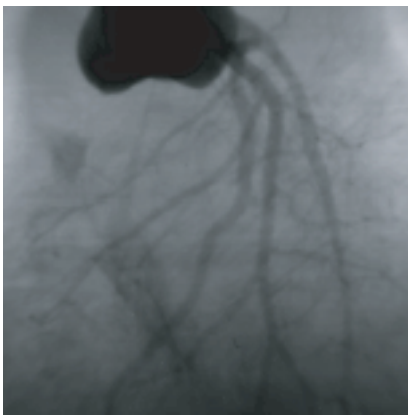

(a) normal image

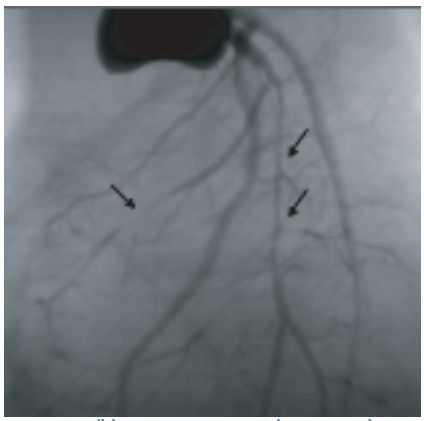

(b) coronary spasm (see arrow)

Figure 4
Imageof rat's coronary arteries.

cular cell or by the dysfunction of endothelial derived vasodilation. This was the first angiographic demonstration of a coronary spasm induced by hyperconstraction in rat. These angiographic results in small animals will be of help to gene therapy research for coronary vasospasm.

Fluorescent X-ray CT

Using fluorescent X-ray CT (FXCT) it was possible to clearly image the distribution of I-127 labeled IMP in the cerebellum of a live mouse (estimated content of iodine in the cerebellum 0.01 mg/g). FXCT has successfully been applied to cerebral perfusion imaging for the first time, indicating that FXCT is siutable for used as a new molecular imaging technique in the near future.

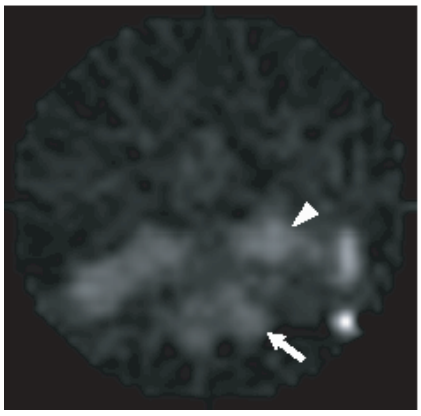

Figure 5
Cerebral perfusion image of a live mouse by fluorescent X-ray CT. Arrow: cerebellum, arrow head: salivary gland uptake of free iodine.

5-9-4 Clinical applications

We have been developing a two-dimensional imaging system for intravenous coronary angiography using monochromatic X-rays at the PF-AR. An advantage of the system is that two-dimensional dynamic imaging of the cardiovascular system can be achieved by using the asymmetrical reflection of a silicon crystal. Initialy four patient examinations were performed in May 1996 using system I. After improvement of the imaging system and the conversion of the NE1A2 hutch to a dedicated hutch for clinical examinations, system II has been employed for clinical examinations since 2000 as a collaboration between the University of Tsukuba and the Institute of Materials Structure Science. Since 2005 images have been obtained using X-ray energies above the K-edge energy of iodine (35 keV) an image intensifier television (II-TV) system and a flat panel detector (FPD). A Schematic diagram of the “Two-dimensional Imaging System II” is shown in Fig. 6.

The photon flux density of monochromatic X-rays transmitted through the lung region is much greater than those traversing the mediastinum. As the dynamic range of the two-dimensional detector (II-TV) is limited, this causes degradation of the vascular diacrisis in the mediastinal region where the coronary arteries overlap other organs such as the aorta and the left ventricle. We have introduced a new method by which the intensity distribution in a two-dimensional irradiation area can be changed by changing the longitudinal size of the electron beam. It is possible to change this intensity distribution quickly using this method. This improvement, along with the high current and long lifetime of the electron beam obtained by efforts of the accelerator group, has made more practical examinations possible. We plan to continue this project to promote its application to clinical evaluation.

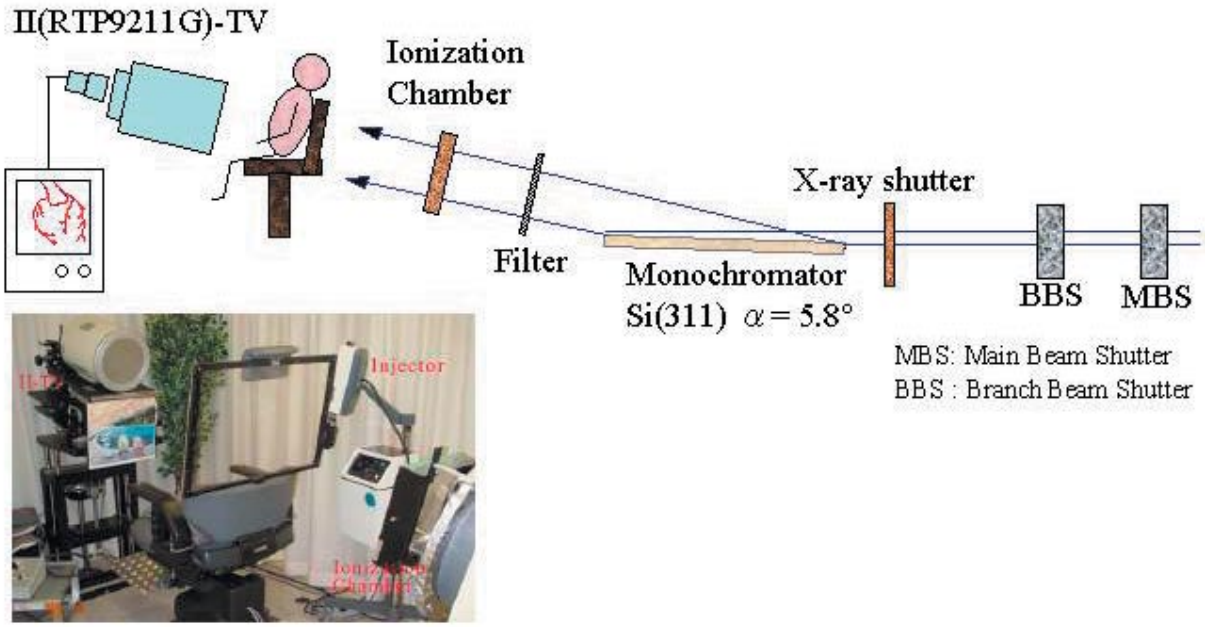

Figure 6
Schematic diagram of Two-dimensional Imaging System II with a picture taken inside the clinical hutch of AR-NE1A2.

(a) (b)

Figure 7
Images of the right coronary artery (arrows). (a) and (b) correspond to the original image and the digital filtered image, respectively (University of Tsukuba).

References

[1] R. Fitzgerald : *Physics Today*, **53 No.7** (2000) 23.
[2] A. Momose : *Jpn. J. Appl. Phys.*, **44** (2005) 6355.
[3] A. Momose, T. Takeda, Y. Itai and K. Hirano: *Nature Med.*, **2** (1996) 473.
[4] A. Yoneyama, T. Takeda, Y. Tsuchiya, J. Wu, Thet-Thet-Lwin, A. Koizumi and K. Hyodo, *Nucl. Instrum. Methods A*, **523** (2004) 217.
[5] T. J. Davis, D. Gao, T. E. Gureyev, A. W. Stevenson and S. W. Wilkins, *Nature*, **373** (1995) 595.
[6] D. Chapman, W. Thomlinson, R. E. Johnston, D. Washburn, E. Pisano, N. Gmur, Z. Zhong, R. Menk, F. Arfelli and D. Sayers, *Phys. Med. Biol.*, **42** (1997) 2015.
[7] V. N. Ingal and E. A. Beliaevskaya, *J. Phys. D*, **28** (1995) 2314.
[8] M. Ando, A. Maksimenko, H. Sugiyama, W. Pattanasiriwisawa, K. Hyodo and C. Uyama, *Jpn. J. Appl. Phys.*, **41** (2002) L1016.
[9] D. Shimao, K. Mori, H. Sugiyama and K. Hyodo, *Jpn. J. Appl. Phys*., **42** (2003) 5874.
[10] K. Hirano, *J. Phys. D, Appl. Phys.*, **36** (2003) 1469.
[11] F. A. Dilmanian, Z. Zhong, B. Ren, X. Y. Wu, L. D. Chapman, I. Orion and W. C. Thomlinson, *Phys. Med. Biol.*, **45** (2000) 933.
[12] I. Koyama, Y. Hamaishi and A. Momose, *AIP Conf. Proc.*, **705** (2004) 1283.
[13] A. Maksimenko, M. Ando, H. Sugiyama and T. Yuasa, *Appl. Phys. Lett.*, **86** (2005) 124105.
[14] J. Miao, P. Charalambous, J. Kirz and D. Sayre, *Nature*, **400** (1999) 342.
[15] J. Miao, K. O. Hodgson and D. Sayre, *PNAS*, **98** (2001) 6641.
[16] K. Hirano, *Trans. MRS-J,* **28** (2003) 43.
[17] K. Hirano, K. Izumi, T. Ishikawa, S. Annaka and S. Kikuta, *Jpn. J. Appl. Phys.*, **30** (1991) L407.
[18] K. Sato, Y. Ueji, K. Okitsu, T. Matsushita, J. Saito, T. Takayama, and Y. Amemiya, *Phys. Rev. B,* **65** (2002) 134408.